Renewable Energy 212 (2023) 138–150

Contents lists available at ScienceDirect

Renewable Energy

journal homepage: www.elsevier.com/locate/renene

Tidal turbine power performance assessments following IEC TS 62600-200 using measured and modelled power outputs

Luke Evans [a,b,*], Ian Ashton [c], Brian Sellar [d]

[a] EPSRC and NERC Centre for Doctoral Training in Offshore Renewable Energy (IDCORE), The University of Edinburgh, Exeter and Strathclyde, Grant Institute Kings Buildings, W Mains Rd, Edinburgh EH9 3JW, UK
[b] European Marine Energy Centre (EMEC), Research Engineer, The Charles Clouston Building ORIC, Back Rd, Stromness KW16 3AW, Orkney, UK
[c] University of Exeter, College of Engineering Mathematics and Physical Sciences, Penryn, Cornwall, UK
[d] The University of Edinburgh (UoE), School of Engineering, Edinburgh, UK

ARTICLE INFO

Keywords:
Acoustic Doppler profiler
Power performance assessment
Power curve
Tidal stream energy
Tidal turbine
ReDAPT
Performance uncertainty
Energy yield
IEC TS 62600-200

ABSTRACT

Demonstrating power performance in real conditions is vital for verifying tidal turbine design. The International Electrotechnical Commission's Technical Specification IEC TS 62600-200 provides guidance for tidal developers to evaluate machine performance. This study evaluates the performance of the operational 1 MW DEEP-Gen IV commercial-scale tidal turbine deployed during the ReDAPT project at the European Marine Energy Centre's tidal test site in Orkney, Scotland. IEC TS 62600-200 states that the power performance should be measured relative to two independently located current profilers deployed in one of two orientations; 'in-line' (preferred) or 'adjacent' (least preferred), relative to the turbine. Two measurement campaigns are used to assess the impact of instrument placement on the measured power curve and annual energy production (AEP). The ambient current flow and vertical profile form differed at each current profiler location (due to topography and bathymetry), leading to AEP variability. The results reinforce the IEC TS preferred orientation for instrument placement, with inline measurements showing smaller variation in AEP estimates compared with adjacent measurements. An additional analysis assesses the sensitivity of AEP estimates on the vertical alignment of the flow profiles with rotor positioning. For this we consider three turbine scenarios: the DEEP-Gen IV and two modelled turbine rotors occupying different regions in the water column. Results show that for regions of high vertical shear, AEP estimates can be misrepresented by up to 5.5% under an imposed vertical misalignment of 2 m. This work has quantified, at this site, the variation in AEP estimates from different flow measurement campaigns informed by IEC TS 62600-200 and has shown the need to ensure good vertical alignment between measurements and turbine rotor positioning.

1. Introduction

Tidal turbine technology is emerging, producing electricity using a renewable and predictable resource. The evaluation of the performance of the tidal turbine in real conditions is challenging and a key factor for the development of this industry to accelerate the commercialisation of current and tidal turbines [1]. The power performance assessment procedure has been described by the International Electrotechnical Commission (IEC) Technical Specification (TS) 62600-200, *"Electricity producing tidal energy converter - power performance assessment"* [2] issued in 2013. However, due to the limited number of tidal energy converters installed on site and producing electricity to the grid, the application of the technical specification by industrials and certification bodies remains limited. Large-scale deployments have occurred in the UK since 2003 [3–7], Northern Ireland in 2009 [8], and France since 2015 [1,9].

The power performance assessment (PPA) of a tidal turbine is a means of relating the current inflow conditions to the output power of the device, leading to the development of a measured power curve. Typically this procedure is undertaken as a key step in achieving type certification of the tidal energy converter (TEC) [4], providing a basis to guarantee the power performance of the device to interested parties, e.g. customers, investors and insurers. Another reason for measuring the power curve is to validate the tools used by turbine designers. Only a few studies have compared theoretical predictions of tidal turbine performance with full-scale measurements, e.g. ReDAPT 2010–2015 [10,11] Deltastreams 400 kW tested in 2015 [4], and Oceanflow

* Correspondence to: 3 Sunnybank drive, Stromness, Orkney KW16 3HS, UK.
E-mail address: Luke.evans@emec.org.uk (L. Evans).

https://doi.org/10.1016/j.renene.2023.05.031
Received 21 February 2022; Received in revised form 29 April 2023; Accepted 4 May 2023
Available online 12 May 2023

Nomenclature

i	Index related to velocity bin
j	Index related to time stamp
k	Index related to current at the depth bin
L	Number of samples in the defined averaging period
n	Index related to data point
S	Number of depth bins across projected area of TEC
z	height from the seabed [m]
$\bar{P}_i$	Mean calculated TEC power in velocity bin i
$\bar{U}$	Mean PWRA velocity, m s^{-1}
$\bar{u}$	Mean velocity, m s^{-1}
$\hat{U}$	Instantaneous PWRA velocity, m s^{-1}
A	Type-A configuration, instrument location, $A1$, $A2$ and $A3$
A_k	Depth bin over the swept area of the TEC, m^2
B	Type-B configuration, instrument location, $B1$, $B2$
C_1	Rotor-Attached instrument
c_s	Speed of sound, m s^{-1}
f_i	Proportion of time during an average year for which the mean current velocity occupies a value within velocity bin i
N_B	Total number of velocity bins in the power curve
U	Mean velocity, m s^{-1}
u	Velocity magnitude, m s^{-1}
z	Height above seabed, m

Energy's 1:10th scale Evopod model [12]. In addition to design verification, monitoring the performance will provide insights on design considerations – machine optimisation and performance deterioration – throughout the lifetime of the device [13,14].

The Reliable Data Acquisition Platform for Tidal (ReDAPT) project commissioned in 2011 provided an extensive amount of operational performance of a 1 MW – Alstom DEEP-Gen IV – full-scale tidal turbine [14,15]. The project objectives were to increase public and industry confidence in tidal turbine technologies by providing a wide range of environmental and performance information [14]. The DEEP-Gen IV performance was evaluated against guidelines published by the IEC TS 62600-200 over a series of deployments at the EMEC full-scale grid-connected tidal test site. This tidal test site has highly energetic tidal currents where the current narrows between the island of Eday and Muckle Green Holm, a small outcrop southwest of the island. The site is depicted in Fig. 1a [10].

The IEC TS 62600-200 [2] requires current velocities to be measured with an Acoustic Doppler Current Profiler (ADCP) during the power performance assessment. Among many configurations, the most common current profiler used in the tidal industry is a diverging beam ADCP in pairs of opposing beams. The position of instruments is to be placed at a large enough distance so that the flow is undisturbed from the operating TEC but not too far to ensure a true representation of the flow characteristics around the TEC location is observed. The position of these current profilers is clearly defined in the technical specification, and the initial influence of these positions has been analysed in Ref. [15]. It recommended further analysis to fully understand the impact of ADCP placement on the power curve.

The current profiler placement is based on a function of the diameter equivalent (D_E) relevant to the proposed TEC. This includes the preferred in-line configuration, which requires the current profiler to be placed between 2 D_E and 5 D_E upstream and downstream of the turbine, and within $\frac{1}{2}D_E$ of the rotor extraction plane centreline laterally, refer back to Fig. 1c. The other option is the adjacent configuration which requires the sensors to be placed between 1 D_E and 2 D_E towards the starboard and port of the turbine extraction plane, and within $\frac{1}{2}D_E$ of the rotor centreline laterally. These guidelines become challenging for turbines with smaller rotor diameters, where the instruments would be placed closer to the TEC, thus potentially observing the effects of pushback flow from the TEC. In extreme cases (5 m rotor diameter), the ADCP location could be close enough to experience interference from reflections of the tidal device. The placement is further complicated if the turbine is on a floating platform subject to sway and surge effects. These motions would reduce the size of the acceptable area in which the current profiler can be placed.

A limited number of studies have looked at the spatial variation in energetic tidal flow conditions using multiple instruments [7,14,16,17]. During the testing of the 1 MW DEEP-Gen IV [15], multiple ADCP campaigns were carried out over two years to measure performance. The results of the campaigns with instruments placed in-line with the TEC suggested that the location of these ADCPs had little significance on the measured performance, even in cases where the ADCP was located outside of the standardised deployment areas [2,14]. However, the deployment of the DEEP-Gen IV found a substantial spatial variation in the cross-stream direction at the Fall of Warness (FoW) [18]. Torrens-Spence [19] conducted a study in the Strangford Narrows (east coast of Northern Ireland), where two instruments were synchronised and attached to two different barges separated by 500 m. The results indicated that the flow characteristics vary significantly due to a rocky outcrop, and flow at each instrument location varied substantially between flood and ebb tides [19], which agrees with work carried out by [18].

Multiple instrument deployments are becoming more common as we aim to gather more in-situ data at tidal test sites to understand the flow characteristics better. In addition, TEC-mounted instruments are being implemented to analyse their capabilities for performance monitoring, with comparisons against traditional seabed-placed instruments considered as the reference. Findings from unique measurement campaigns with standardised placed instruments and an operating full-scale commercial TEC can help provide insights and re-inform standardised methods [4,10,15,20].

Many TEC designs exist, all having different characteristics (e.g. rated power and rated velocity) and deployed at different depths (z) along the water column. For turbines that float, the motion from mooring cables, in addition to the flow velocity in the upper regions of the water column, adds further complexity to carrying out a power performance assessment. The floating TEC concept is likely exposed to further tidal flow variation due to wind-induced flow and wave–current interaction, and measured flow data is frequently removed close to the surface. This can impact the calculation of the power-weighted rotor average (PWRA) velocity, recommended in the IEC TS 62600-200. Furthermore, capturing the orientation and location of the current profiler become difficult once it is lowered into the water. Increasing the accuracy of sensor deployment position and orientation comes with additional costs, and can involve the use of further dedicated sub-systems and complex installation techniques. As such, quantifying the impact of spatial variability and verifying the use of TEC-mounted measurements can help expand the acceptable PPA instrument configurations.

To date, the IEC TS 62600-200 does not recognise TEC-mounted instruments that profile in the horizontal plane. Harrold et al. [4] compared recorded power measurements with theoretically predicted measurements from Tidal Bladed. These predictions were compared using measurements from the rotor-attached single-beam acoustic Doppler

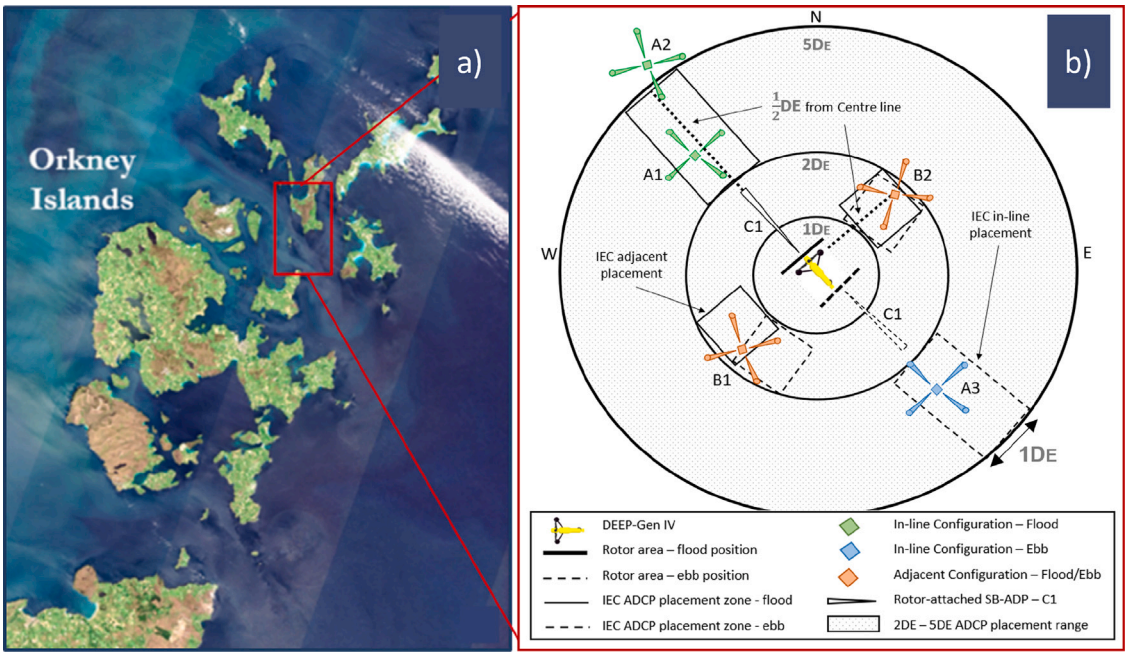

Fig. 1. Map showing (a) the Orkney Islands, Scotland, and the location of the European Marine Energy Centre (EMEC) tidal energy test site (red rectangle). The plan view of the measurement campaign is presented in (b), where the IEC TS 62600-200 highly influences the instrument placement and is placed relative to the DEEP-Gen IV [2]. A1, A2, A3, B1 and B2 are seabed current profilers, and C1 is a rotor-attached current profiler.

profiler (SB-ADP) and a seabed-mounted ADCP. The observations found that the TEC-mounted instrument corresponded closely to theoretical predictions from the industry standard tidal turbine modelling software Tidal Bladed, which provides accurate numerical load and performance estimates. However, the SB-ADP consistently measured weaker flows due to a spatial variation between instrument locations [4]. Instruments mounted on TECs limit the requirement for seabed ADCPs for power performance, thus providing flexibility for PPA and reducing additional costs of offshore deployments.

This paper aims to highlight the effect of ADCP placement (per the IEC TS 62600-200) on the power performance assessment of an operational 1 MW tidal turbine. We investigate the variation in velocity based on in-situ data obtained from two measurement campaigns – five separate current profilers – deployed at the FoW (Orkney, Scotland). The paper is structured as follows: Section 2 provides a test overview of the installation site, tidal turbine, the suite of instruments relative to this study, and the post-processing of the in-situ measurements; Section 3 reports on the key results obtained for the difference between an inter-instrument comparison (3.2), spatial variation in velocity (3.3) and the impact of instrument placement on the measured power curve 3.4. In addition, consideration of the vertical misalignment between the instrument measurement and the TEC hub-height and the effect this has on the estimated AEP is presented in (3.5). Section 4 discusses these key findings in the context of existing best practices; while Section 5 summarises this work to form a conclusion.

2. Test overview

2.1. Deployment site conditions

All the instruments and the TEC were deployed in Berth 2 at the FoW, at a depth of ≈ 43–46 m, see Fig. 1a for a high-level location of the tidal test site and 1b for a plan view of the measurement campaigns. The bathymetry of a TEC test site must be surveyed to ensure that it is free from obstacles and topography that could affect the performance of the TEC. Therefore, a rectangle box (10 D_E × 20 D_E) was surveyed for the PPA as per the IEC TS 62600-200, see Fig. 2a, b.

Table 1
Key parameters of the DEEP-Gen IV TEC.

Developer	Units	Alstom
Type	–	3-Blade HATEC
Foundation	–	Piled tripod
Production year	–	2011
Distance above seabed	m	18 (hub-height)
Blade radius	m	9
Projected capture area	m^2	256.74
Rated output power	MW	1
Cut-in	m s^{-1}	1
Rated speed	m s^{-1}	2.7
Nominal rotor speed	rpm	13.78
Maximum rotor speed	rpm	19.29

The depth within the 10 D_E × 20 D_E area ranges from 46 m northwest of the turbine, to 39 m near the east side of the area of interest. The latter is considered far enough from the turbine to create any significant disturbance in the turbine flow. The directionality and strength of typical tidal currents (from the five seabed placed instruments) at the deployment location are shown in Fig. 3.

The tidal currents at the site are predominantly bi-directional with an offset of ≈ 45° from North/South. The ebb tide is stronger at this location, reaching mean flows up to 4 m s^{-1}, whereas the flood tide reaches ≈ 3.5 m s^{-1}. The ebb tide is also much more turbulent due to the flow being disturbed by several features of the site bathymetry and local islands, which has been reported on by others [22,23].

2.2. Turbine description

The tested turbine is a 1 MW rated machine with a three-bladed, 18 m diameter, variable-pitch, horizontal-axis rotor. Other key parameters are presented in Table 1. The turbine typically yawed between flood and ebb tide (rotating during slack tides) so that the energy extraction plane is perpendicular to the established flow direction commonly refereed to as the principle flow direction. Outline turbine parameters are listed in Table 1.

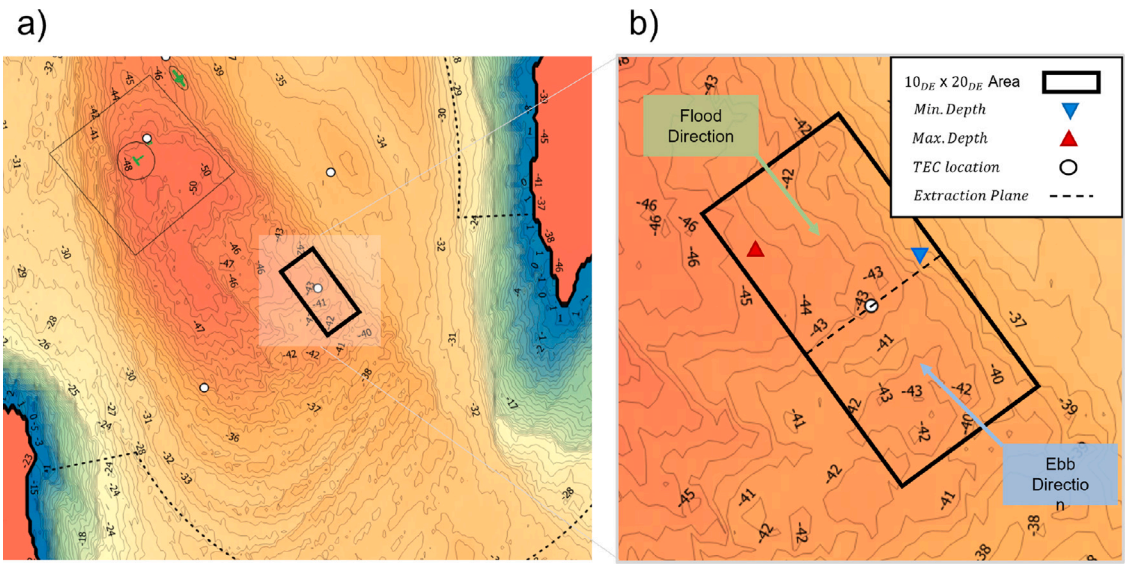

Fig. 2. Bathymetry in the vicinity of the turbine, with (a) showing the 10 D_E × 20 D_E area of interest (solid black rectangle within highlighted grey squared), and (b) a closer view at the depth around the DEEP-Gen IV. 'Contains Maritime and Coastguard Agency data © Crown Copyright' [21].

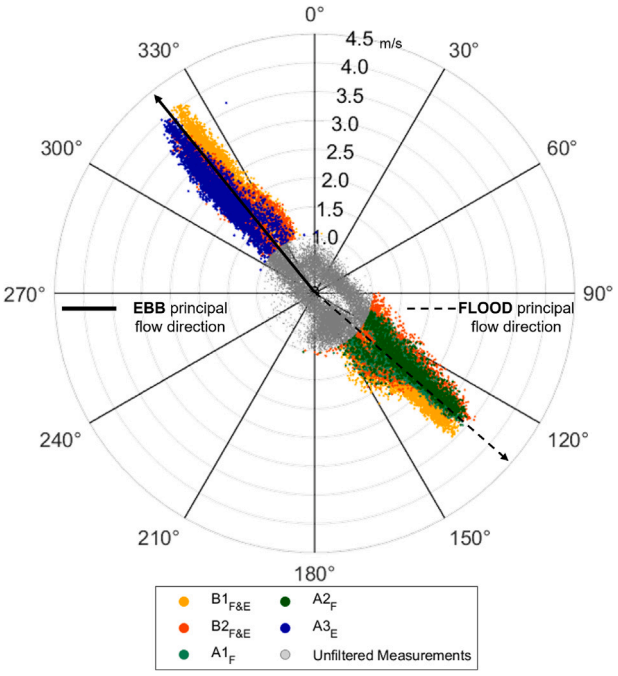

Fig. 3. Directionality and strength of the flood and ebb tidal characteristics at Fall of Warness at each instrument location used in the analysis.

2.3. Instrumentation

A summary of the suite of instruments used is provided in Table 2, and their approximate locations are shown in Fig. 1c. Two measurement campaigns are considered, deployment 5 (in-line with TEC, denoted "*A*"), contains three seabed ADCPs, depicted as *A*1, *A*2, *A*3, and deployment 6 (adjacent to TEC, denoted "*B*"), contains two seabed ADCPs, *B*1 and *B*2, see Fig. 4 for a visual representation. These measurement campaigns are chosen as they are placed within the two stated zones recommended by the IEC TS, with the addition of an extra instrument placed in-line but just outside the IEC TS target placement zone.

Table 2
Key parameters of acoustic current Doppler profilers (ADCP) used in the flow characterisation.

Identification/s	*A*1, *A*2, *A*3 *B*1, *B*2	*C*1
Instrument	WHS	AD2CP
Manufacturer	RDI	Nortek
Acoustic frequency	600 kHz	1000 kHz
Type	ADCP	SB-ADP
Sample rate	0.5 Hz	2 Hz
Quantity	5	1
Location	Seabed	RA
No. operating beams	4	1
Bin length	1 m	0.5 m

RA = Rotor-Attached.

The single-beam flow profiler (SB-ADP) was used throughout both deployments, attached to the Alstom DEEP-Gen IV's rotor (*C*1). This data set allows comparison between the two IEC TS recommended orientations to a TEC-proximal location. Orientation *A* had two ADCPs (*A*1, *A*2) measuring concurrently at locations upstream of the TEC (on a flood tide), separated by 45 m. The SB-ADP measurements were compared with the seabed instruments to assess the capabilities for performance assessments. Data collected from the two deployments (*A*&*B*) included periods of spring and neap tides. The data used in the analysis for type *A* and *B* are ≈ 15 and ≈ 57 days long, respectively. Table 3 provides relevant measurement campaign information.

The location of the ADCPs was known to the nearest metre based on their UTM coordinates, see Table 3. Using a bathymetric map in conjunction with each ADCP pressure data, their depths relative to the TEC were estimated to the nearest metre (as the instruments have a resolution of 1 m), see Fig. 1b. Velocity variation along the depth bins was analysed.

A 2° tilt on the TEC base led to a variation in depth which altered the horizontal bin ranges of *C*1. At 12 m, a maximum difference of 0.42 m was found. In addition to the TEC tilt, the turbine was manually rotated about its yaw axis to match the incident flow direction, but this process was inaccurate. As *C*1 faced the direction of the TEC yaw angle, it was often not aligned to the principal flow direction, thus measuring a minor component of the current velocity.

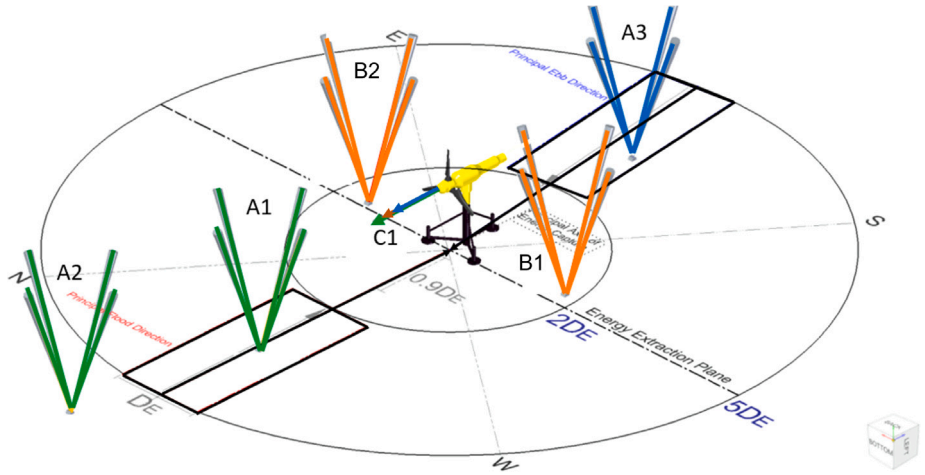

Fig. 4. Instrument placements for deployments 5 and 6 showing distance (DE) from the DEEP-Gen IV TEC, relative to North. Generated data-sets from Deployment 5 are identified as $A1$, $A2$ and $A3$ targeting ambient conditions on the flood (green beam) and ebb (blue beam) tides, respectively. Deployment 6 featured $B1$, $B2$ data-sets (orange beam) targeting ambient flows on both the flood and ebb tide. The rotor-attached (hence yawing with the TEC) single-beam instrument, $C1$, measured both flood and ebb tides.

Table 3
Turbine-proximal deployments of ADCPs showing unique campaign ID, date deployed (date format yyyy-mm-dd) and deployment duration. The coordinate system is WGS84.

ADCP ID	Seabed Campaign ID	Deployed	Recovered	Days	LocationNorth [°]	LocationWest [°]
A1	ADCP01_NW_Dep5	2014-06-22	2014-08-05	41	59.13726	2.80651
A2	ADCP02_NW_Dep5	2014-07-07	2014-08-16	40	59.13764	2.80686
A3	ADCP03_SE_Dep5	2014-07-07	2014-08-17	41	59.13643	2.80529
B1	ADCPTD7_01_Dep6	2014-09-17	2014-12-11	85	59.13705	2.80526
B2	ADCPTD7_02_Dep6	2014-09-17	2014-11-27	71	59.13667	2.80641
C1	SBD01	2014-06-23	2014-12-21	85	59.13685	2.80583

2.4. Instrument data processing

2.4.1. Data quality control (QC)

Data quality control (QC) was implemented on the ADCP and SB-ADP data. Recommended QC measures were based an internationally-recognised guideline, QARTOD, and instrument manufacturer recommendations, [24–26]. First, an excessive tilt threshold of <−15° and >15° was applied to both pitch and roll data. Secondly, a speed of sound (SoS) threshold of <1470 m s^{-1} and >1570 m s^{-1} was applied. The signal-to-noise (SNR) measures the signal's amplitude over the background noise level. Amplitude thresholds have been chosen to reject data from beyond the normal operating range of each instrument: a threshold of < 64 dB was applied for SNR based QC for the ADCPs. Lastly, a signal correlation threshold was applied. Values which correspond to a correlation <70% were flagged. A de-spiking algorithm was applied to detect velocity outliers, which flagged all values with a change of 1 m s^{-1} between consecutive samples. Data points that were flagged in these QC steps were removed.

During the processing stage, shear profiles were plotted for all five seabed-placed ADCPs. Data quality was found to deteriorate close to the sea surface. Therefore the top 6% of current depth bins were removed as recommended by RDI [25], for a 20° ADCP slant angle.

The SB-ADP measured the current flow along the beam with a manually set speed of sound value of 1470 m s^{-1} and required an SoS correction to match the seabed-placed ADCP, specifically $A1$ for the in-line orientation and B_1 for the adjacent orientation. This was accounted for during data processing via scaling, as per Eq. (1):

$$u_{C1} = u_{C1_{(org)}} \cdot \frac{S_{A1}}{S_{C1}} \tag{1}$$

where u_{C1} is the corrected instantaneous velocity, $u_{C1(org)}$ is the uncorrected instantaneous velocity measured by C_1, S_{A1} is the instantaneous SoS reported by the ADCP, S_{C1} is the manually set SoS for the single-beam ADP.

The difference in the measured current velocity between u_{C1} and U_{A1} due to TEC misalignment to the principle flow direction was considered negligible at less than 0.25%. In addition, the velocity measured along the SB_{C1} beam, with the horizontal axis tilt considered, was equivalent to the cosine of 2° and was also considered negligible at less than 0.1%.

2.4.2. Turbine mounted single beam profiler

The SB-ADP data was used to monitor the rotor approach flow using the approach carried out by [4,27]. Minimum variation in the longitudinal flow velocity was observed between ≈ 10–12 m for $C1$. Flow deceleration occurs closer to the TEC as the flow expands around the rotor, and at distances greater than 17 m severely decreased flow is observed. This is directly related to the instrument range capabilities, where the SNR increases. The region of highest data reliability was between 10–12 m, therefore, u_{C1} was spatially averaged, hereafter referred to as $\bar{u}_{C1}$, and representing the longitudinal velocity reference for the TEC mounted instrument ($C1$, refer to Fig. 4).

2.4.3. Power-weighted rotor average (PWRA) velocity

The instantaneous power-weighted rotor average (PWRA) velocity was calculated for the five seabed-placed ADCPs. This was achieved by averaging the velocity measurements from the 19 depth bins corresponding to the rotor plane. Greater weighting was applied to the bins closest to the rotor hub centre, where the swept cross-section area is the largest, as per Eq. (2):

$$\hat{U}_{i,j,n} = [\frac{1}{A}\Sigma_{k=1}^{S} u_{i,j,k,n}^{3} A_k]^{\frac{1}{3}} \tag{2}$$

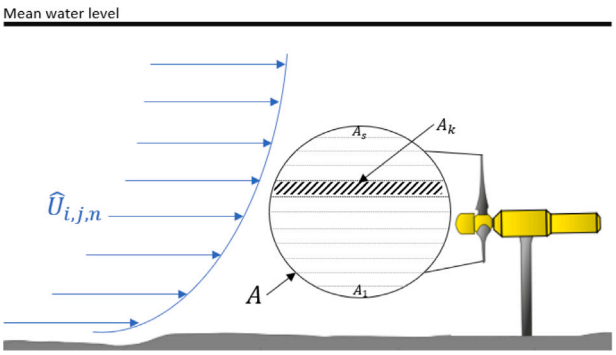

Fig. 5. Power weighted rotor average velocity example.
Source: Image adapted from [2,29].

where $\hat{U}_{i,j,n}$, is the instantaneous PWRA velocity, A_k is a depth bin over the swept area of the TEC rotor, $u^3_{i,j,k,n}$ is the velocity in the relative bin, and i, j, k, are index numbers for the velocity bin (increments of 0.1 m s^{-1}), time instant of the measurement and the current depth bin across the projected capture area, respectively, see Fig. 5 for visual representation. The in-situ measurements were then averaged by an integer divisor of 10 minutes, in this case, 5 minutes. Where $\hat{U}_{i,j,n}$ should be averaged to produce the mean PWRA velocity, as shown in Eq. (3) below:

$$\bar{U}_{i,n} = [\frac{1}{L}\Sigma_{j=1}^{L}\hat{U}^3_{i,j,n}]^{\frac{1}{3}} \quad (3)$$

where L is the number of samples in the defined averaging period, and $\bar{U}_{i,n}$ is the mean PWRA velocity in velocity bin i for data point n in m s^{-1}. The method of calculating the PWRA velocity can lead to inaccuracies if the wrong reference depth is chosen. This is not addressed in the current work. However, a detailed power curve of DEEP-Gen IV during the October 2013 campaign [28] showed that this accounts for approximately 2% uncertainty in the velocity. The current velocity data exceeded 15 days of measurements, where each velocity bin increment of 0.1 m s^{-1}, i, contained at least 30 minutes of in-situ data (as per IEC TS 62600-200).

2.4.4. DEEP-gen IV power data

Power measurements were available and used in this analysis for the DEEP-Gen IV (TEC case 2). The two deployment campaigns, A and B, featured periods with no generated power from the DEEP-Gen IV and periods of inconsistent power generation. The time-matched current velocities for these periods where the turbine produced no power were removed from the analysis.

Table 4 illustrates the inter-instrument comparison and the number of 5-minute samples available after QC and filtering the data for periods of no power generated by the DEEP-Gen IV. Instruments used for the flood tide comparison are as follows: $A1$, $A2$, and $C1$ for the in-line measurements, and $B1$, $B2$, and $C1$ for the adjacent. Instruments used for the ebb tide comparison are as follows: $A3$ and $C1$ for the in-line measurements, and $B1$, $B2$, and $C1$ for the adjacent.

2.4.5. Alternate turbine types

In order to assess the impact of vertical misalignment on energy production, two further turbine types are introduced, labelled case 1 and case 3, using modelled power (as opposed to measured power as was the case with the DEEP-Gen IV). The turbines used for case 1 and case 3 are based on deployed variants of horizontal axis tidal turbines that occupy different regions in the water column. They are informed by the RealTide project [30], with basic parameters provided in Table 5. Where z relates to the hub-height of each turbine above the seabed, and C-S is the cross-sectional area of their rotors. Since the measurements used for this case study focus on the instruments

Table 4
Inter-instrument comparison table showing number of available 5-minute ensembles, where colours correspond directly to instruments depicted in Fig. 4. The light grey shaded region corresponds to flood conditions with data relating to ebb shown diagonally opposite.

ADCP ID	A1	A2	A3	B1	B2	C1
A1	x	x	x	x	x	x
A2	2172	x	x	x	x	x
A3	x	x	x	x	x	4579
B1	x	x	x	x	8458	8458
B2	x	x	x	9646	x	8458
C1	2172	2172	x	9646	9646	x

Ebb Conditions

Flood Conditions

Table 5
Generic types of tidal energy converter parameters.

TEC characteristics	Units	Case 1	Case 2	Case 3
z	m	12	18	34
Rotor Diameter	m	12	18	20
C-S Area	m^2	113.1	254.5	314.2
Rated Power	MW	0.1	1	2

placed adjacent (B) to the DEEP-Gen IV location, the turbine does not affect the measurements collected. Therefore, the two additional turbines will be "in theory" at the same location as the DEEP-Gen IV. The impact of vertical alignment between the instrument and TEC hub-height can then be assessed for three turbines which experience different variations of shear in the water column.

The 5-minute time-average velocities U_{B1} and U_{B2}, were used to measure vertical misalignment error between the ADCP depth bin and the TEC rotor plane, as both instruments measured the flood and ebb tide. The current velocities taken at the hub-height of the proposed TEC concepts were used. Calculating the PWRA velocity was not possible for the floating TEC concept due to the removal of data in the upper region of the water column (refer back to Section 2.4.1). The alignment error was analysed in increments of 1 m up to ± 2 m from the hub-height.

2.4.6. Estimated annual energy production

The Annual Energy Production (AEP) estimates were derived using real world power generated from the DEEP-Gen IV, this is used in Sections 3.4 and 3.5 where the DEEP-Gen IV analysis forms case 2. The modelled power – produced from velocity measurements at locations B1 and B2 and theoretical turbine parameters – was used in Section 3.5 forming cases 1 and 3. Power data was time-integrated (using MATLAB trapezoidal method) and scaled by the ratio of measurement duration with respect to the number of days in a year, as per Eq. (4):

$$AEP = R \cdot \Sigma_{t1}^{t2}\bar{P}dt \quad (4)$$

where AEP is the expected annual energy production in MWh, R is the ratio of the number of days in a year over the duration of the campaign, $\bar{P}$ is the 5-minute averaged measured TEC power, t_1 is the index number defining the time start, t_2 is the index number of the end time interval.

For cases 1 and 3 (selected as representative of current technologies) which lack real-world data, two pre-defined power curves of rated power 0.1 MW and 2 MW were produced using Eq. (5):

$$\bar{P} = P_{rated} \cdot \left(\frac{V^2 - V_{ci}^2}{V_r^2 - V_{ci}^2}\right) \quad (5)$$

where P_{rated} is the predefined rated power, V is the velocity measurement, V_{ci} is the cut-in velocity for the proposed TEC, and V_r is the rated velocity for peak power production. In both cases power was capped at the corresponding rated power.

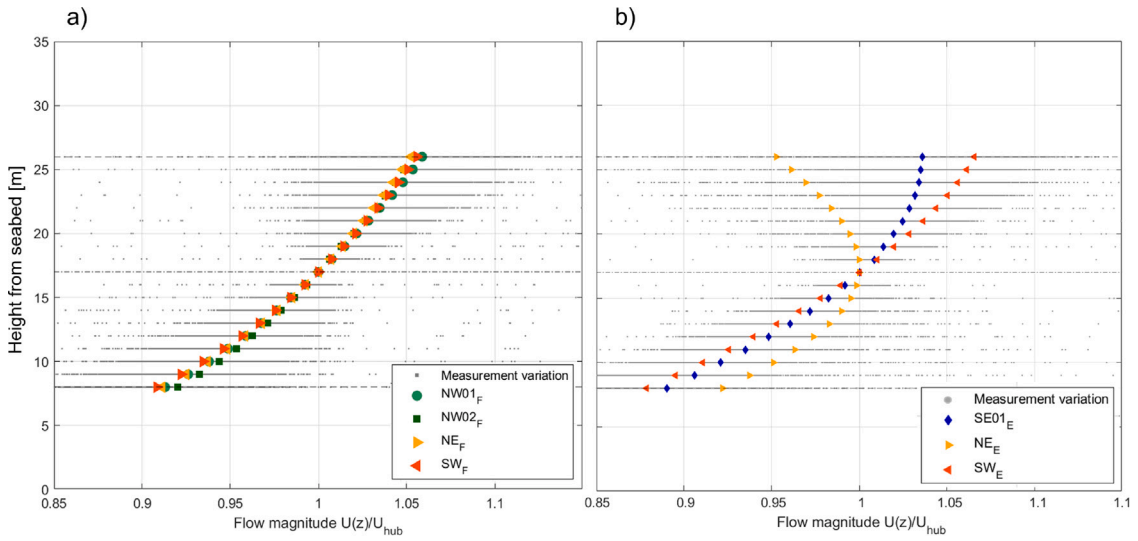

Fig. 6. Current velocity across the rotor plane for the DEEP-Gen IV, normalised by the hub-height at 18 m. The current velocity refers to the measurements captured for (a) flood tide, and (b) ebb tide. Approach adapted from Harrold et al. [4].

3. Results

3.1. Preliminary analysis of ADCPs

Five tidal ellipses were produced (refer back to Figs. 3, and 4) to show how the strength and direction of the flow vary per instrument location. As can be seen in Fig. 3 at this location the ebb tides are faster than the flood tides by ≈ 0.8 m s^{-1} and the tides are ≈ 10° off from being rectilinear. There is some disagreement in the principal flow direction amongst the ADCPs. In the flood tide, these disagree by as much as 10°, whilst the difference is closer to 5° in the ebb direction. The calculation of PWRA velocities are insensitive to flow direction since they involve velocity magnitudes. However, for other applications, e.g., turbine operation and control, directionality should be considered.

3.2. Inter-instrument comparison

The current velocity measurements at a range of heights covering the TEC rotor plane from instruments placed at locations *A* and *B* (refer back to Fig. 4) are presented in Fig. 6. Velocities were normalised by hub-height velocities (18 m above seabed for the DEEP-Gen IV TEC). These are compared against a mean velocity profile. The instruments were compared based on placement and tidal cycle. The in-line current velocity, measured by U_{A1} ($NW01_F$), and U_{A2} ($NW02_F$) varied by ≈ 0.75% at the lower bounds, and ≈ 0.35% at the upper bounds. Similarly, U_{B1} (SW_F) and U_{B2} (NE_F) differed by alike margins during the flood tide, Fig. 6a. In contrast, the ebb tide revealed a substantial variation along the rotor plane, where U_{B1} and U_{B2} record significantly different current velocities in both the most-lower bound and most-upper bound, differing by ≈ 5%, and ≈ 12% respectively. Similar velocity reductions have been found in the upper region of U_{A3}, see Fig. 6b.

Fig. 7 displays the correlation between time-matched velocities for each instrument pairing, where the in-line instruments A_1, A_2 are ≈ 45 m apart, and the adjacent instruments B_1 and B_2 are ≈ 70 m apart. The sum of square error (SSE) and the root mean squared error (RMSE) of the relationship between compared instruments is shown in Fig. 7.

The flood tide velocity measurements $\bar{U}_{A1}$, $\bar{U}_{A2}$ and $\bar{U}_{B1}$ $\bar{U}_{B2}$ show high correlation. However $\bar{U}_{B1}$ and $\bar{U}_{B2}$ contain a lot more data scatter with a larger SSE when compared with $\bar{U}_{A1}$ and $\bar{U}_{A2}$ as shown in Fig. 7a. Unlike the flood tide, the ebb tide was measured by a single ADCP, A_3. This was compared with C_1, indicating a strong correlation (with an RMSE comparable with the other in-line instruments A_1, and A_2 measuring the flood tide). However, a clear bias is present, where C_1 consistently underestimates the velocity compared with the traditional seabed-placed A_3, which is in agreement with previous work [15,27], refer to Fig. 7b. The ebb tide velocity scatter from B_1 and B_2 comparisons is also shown in Fig. 7b, with greater variation than the equivalent comparison on the flood tide. This scatter increases further at higher velocities, where B_2 measurements also trend towards slower velocities.

3.3. Spatial variation in velocity

Velocity profiles were produced to analyse how the flow changes with depth. The measurements of velocity from instruments in both configurations *A* and *B*, were split by flood and ebb tides and subdivided into velocity bins in increments of 0.3 m s^{-1}. It can be seen in Fig. 8a that the difference between U_{A1} and U_{A2} at hub-height and the speed of rated power (1 MW) is 0.5% for the instruments placed in-line measuring the flood tide. Fig. 8b shows larger differences between the equivalent measurements for the *B*1 and *B*2 pairing, at 3.1%.

The velocity measured by the rotor-attached hub-height SB-ADP, $\bar{u}_{C1}$, is shown as a filled circle. The instrument measured a reduced velocity, commonly close to ≈ 0.15 m s^{-1} slower than U_{A1}, U_{A2}, U_{B1} and U_{B2} during the flood tide.

Ebb tide data presented in Fig. 9b shows a larger discrepancy between U_{B1} and U_{B2}. Differences increase with higher velocity and height above the seabed. At the rated-power velocity of 2.7 m s^{-1} differences ranged from 2.1–19.4% from the bottom-most and top-most locations respectively of the rotor plane. $\bar{u}_{C1}$, shown as filled circles, corresponds closely with U_{B2} for the ebb tide measurements.

3.4. Power curve and AEP comparison

The velocities from each seabed ADCP and the rotor-attached SB-ADP were paired with the real-world power measurements from the DEEP-Gen IV, and then sorted into velocity bins in increments of 0.1 m s^{-1} in accordance with the IEC TS 62600-200. The mean velocity flow and power within each bin were then calculated. Fig. 10 presents the final power curves for the flood and ebb tide. The black solid line shows the power curve provided by the DEEP-Gen IV operator, Alstom [28]. The measured power curve was produced with reference to the velocity measured at C_1. This curve implies the DEEP-Gen IV produced more power under slower flow velocity conditions when

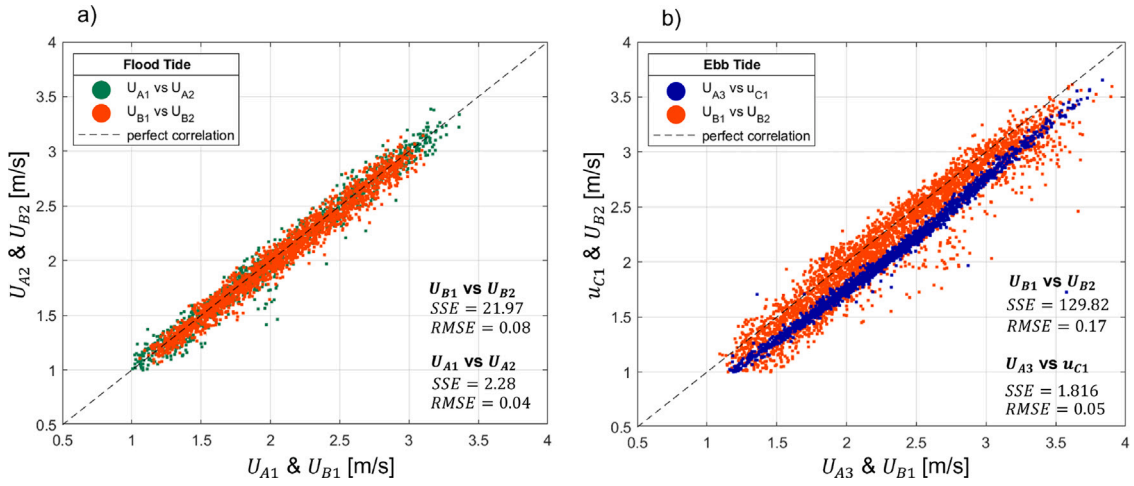

Fig. 7. (a) Inter-instrument correlation for the flood measurements, $\bar{U}_{A1}$ vs $\bar{U}_{A2}$ (green) and $\bar{U}_{B1}$ vs $\bar{U}_{B2}$ (orange). (b) Ebb tide correlation, for $\bar{U}_{A3}$ and $\bar{u}_{C1}$ (blue), and $\bar{U}_{B1}$ vs $\bar{U}_{B2}$ (orange).

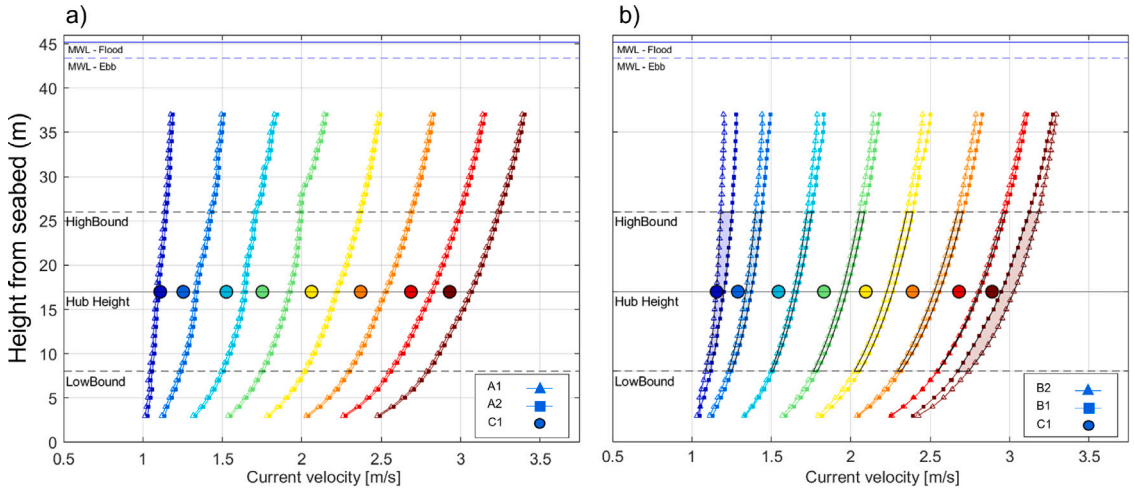

Fig. 8. Velocity depth profile for flood tide measurements for (a) in-line ADCP pair A_1 and A_2, compared against the rotor-attached instrument C_1 (filled circle marker at hub-height, 18 m). (b) Velocity measurements from the adjacent locations to the TEC B_1 and B_2, the rotor-attached SB-ADP C_1 is depicted as a filled circle at hub-height.

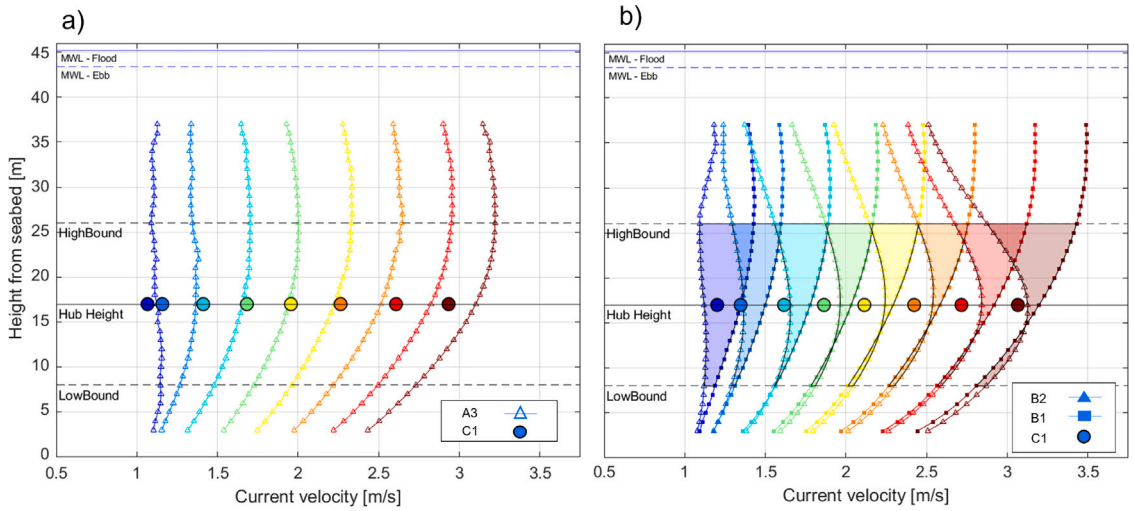

Fig. 9. Velocity depth profile for ebb tide velocity measurements for (a) in-line ADCP A_3, and SB-ADP C_1 (filled circle marker at hub-height of 18 m). (b) Velocity measurements from the adjacent locations to the TEC, B_1 and B_2, and the rotor-attached SB-ADP C_1.

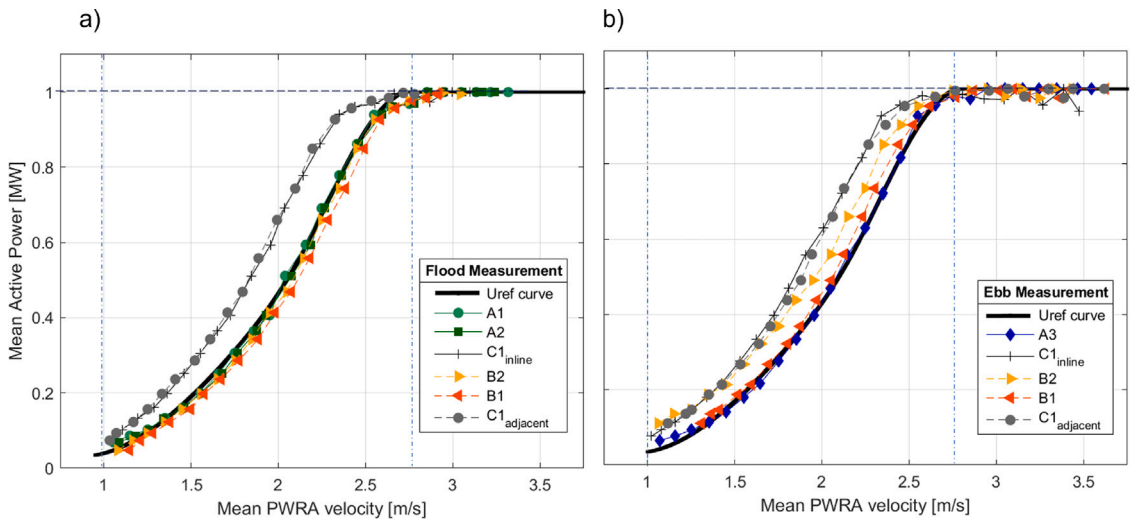

Fig. 10. The effect of ADCP placement – per IEC TS 62600-200 – on measured power curve for the averaged 5-minute velocities in increments of 0.1 m s^{-1}. (a) The flood tide measurements from the in-line ADCP pair $\bar{U}_{A1}$ and $\bar{U}_{A2}$, the adjacent pair are included $\bar{U}_{B1}$ and $\bar{U}_{B2}$. (b) The ebb tide measurements from the rotor-attached SB-ADP, $\bar{u}_{C1}$ and $\bar{U}_{A3}$, and the adjacent pair $\bar{U}_{B1}$ and $\bar{U}_{B2}$. The black line represents the published power curve of the DEEP-Gen IV [28].

compared with velocity measurements at the seabed-placed ADCP locations. However, the velocity measured by the rotor-attached SB-ADP was shown to underestimate the flow approaching the rotor (Figs. 7b and 8). Therefore, the power curve is misleading and implies the SB-ADP provides a more favourable power curve from a developers perspective. A key part of this study is to assess the impact of using ADCPs around the extremities of the IEC TS target locations. For this, the measured power curves for the flood tide measurements are shown in Fig. 10a. The mean velocity at rated power (1 MW) for ADCP pair $\bar{U}_{A1}$ and $\bar{U}_{A1}$ (approximately 3.4 D_E and 5.5 D_E from the rotor centre respectively) differ by 0.6%. Whereas, the mean velocity at rated power for ADCP pair $\bar{U}_{B1}$ and $\bar{U}_{B2}$ (located 32 m southwest and 34 m northeast of the rotor centre) differed by 1.1%.

The ADCP pair positioned in-line A_1 and A_2, measure a slightly lower velocity compared with the ADCPs positioned adjacently B_1 and B_2. From a developer perspective, this results in a seemingly more efficient power curve when a lower mean velocity, U_{A1}, is compared with the higher mean velocity, U_{B1}, for the equivalent power. Fig. 10b shows the power curves for the mean velocities measured for the ebb tide by: in-line ADCP A_3; adjacent ADCP pair B_1 and B_2; and the rotor-attached SB-ADP C_1. At the lower velocity increments (<2 m s^{-1}) there are more obvious difference between the three curves produced from $\bar{U}_{A3}$, $\bar{U}_{B1}$ and $\bar{U}_{B2}$. This is likely due to a combination of faster accelerations in this regime and a spatial variation in the measured velocity on the ebb tide. At rated power, the ebb tide curves produced by $\bar{U}_{B1}$ and $\bar{U}_{B2}$ differ by 4.3%.

In terms of the flow references measured by ADCP pairs A_1 and A_2, and B_1 and B_2, a better agreement with the predicted curve is found using the ADCPs placed in-line to the TEC. This is shown for the ebb tide power curves, where A_3 is placed in-line and closely matches the predicted curve of the DEEP-Gen IV. It is likely that these findings highlight that there are periods in which the seabed ADCPs placed adjacent do provide a good reference velocity (velocity increments < 1.5 m s^{-1}), but differences grow between ADCP pair placed in-line and ADCP pair placed adjacent as the mean velocity increases at the site.

In addition to the measured power curves generated from seabed ADCPs, the SB-ADP flow measurements are used to assess the power curve. Unlike the ADCP datasets however, there is no accounting for the vertical variation or directionality in the flow and so the SB-ADP represents a hub-height speed along the axis of rotation. Velocities for each seabed ADCP were compared against the velocity measured at C_1. The velocity differed by up to ≈ 8% when compared with ADCPs positioned in-line A_1 and A_2, and 11% when compared with ADCPs positioned adjacently B_1 and B_2.

Annual Energy Production was estimated using the pre-defined power curve provided by Alstom for the 1 MW DEEP-Gen IV. The PWRA velocities, measured at locations *A* and *B* relative to the TEC location and hub-height, were paired with the corresponding power via a look-up table to form a power time-series. In terms of the two orientations – in-line and adjacent – a better agreement between ADCP pair A_1 and A_2 was found. Fig. 11 shows the variation in velocity between instrument pairs calculated at various velocity bins. It can be seen that differences reduce during faster flows (where the turbine generates most of its power). The AEP differed by 1.2% between A_1 and A_2, and 2.6% between B_1 and B_2 for the flood tide. The ebb tide, measured by ADCPs at B_1 and B_2 differed by 7.3%.

3.5. Impact of vertical misalignment between measurements and TEC rotor plane

An additional analysis on the impact of flow measurement vertical misalignment was conducted on three types of TEC: the ReDAPT commercial-scale tidal turbine, and two further variants of horizontal axis tidal turbines (selected as representative of current technologies), which operate in different locations of the water column. The ADCPs placed adjacently - B_1 and B_2 - to the DEEP-Gen IV are used to assess the sensitivity to the vertical alignment, see Fig. 12 and Table 6.

The streamwise velocity varies with increasing height from the seabed, typically following a logarithmic curve. The hub-heights for each TEC (refer to Table 5) were used as the base case, and depth bins (ranging in 1 m) up to ± 2 m from the hub-height were assessed. The difference from a positive shift (towards the sea surface) in the bin resulted in an overestimation of AEP. On the contrary, a negative shift (towards the sea floor) is related to underestimating the total AEP. The results are summarised below:

1. With an imposed vertical misalignment of 2 metres between measurement locations and modelled rotor plan differences for flood and ebb tides, respectively, are up to 4.5% and 5.5%.
2. The variation in AEP estimated from the flood tide velocity measurements were similar at locations B_1 and B_2 for a misalignment up to 2 m, implying that the vertical variation in U_{B1} and U_{B2} for the flood tide are similar across a distance of ≈ 70 m.

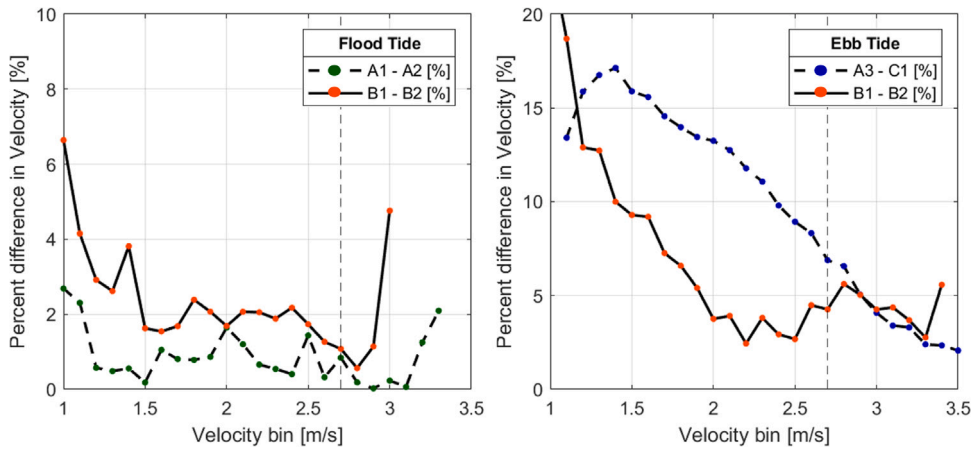

Fig. 11. In-line placed ADCPs (black dashed line) A_1, A_2, A_3 and adjacent placed ADCPs B_1, B_2 (black solid line) and their calculated PWRA velocity in increments of 0.1 m s^{-1}. (a) Flood tide PWRA velocity difference between pair: $\bar{U}_{A1}$ and $\bar{U}_{A2}$, and pair $\bar{U}_{B1}$ and $\bar{U}_{B2}$. (b) Average velocity difference between $\bar{u}_{C1}$, $\bar{U}_{A3}$, and the PWRA velocity difference between $\bar{U}_{B1}$ $\bar{U}_{B2}$.

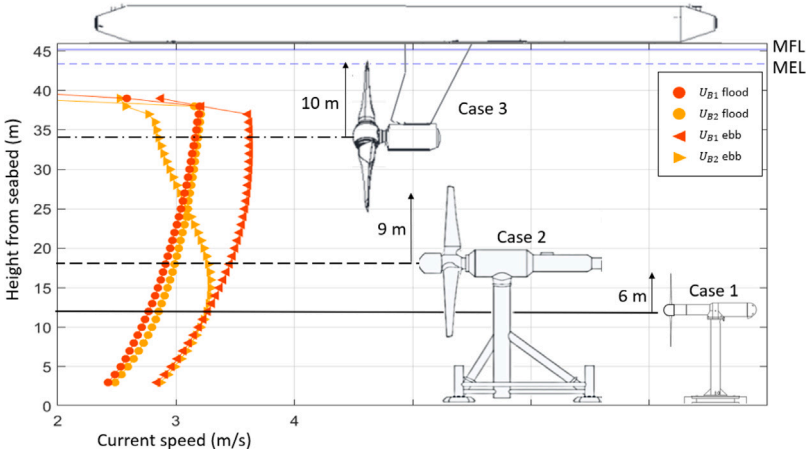

Fig. 12. Three TEC concepts are placed accordingly to their hub-height reference. U_{B1} and U_{B2} represent the peak rated velocity for the flood and ebb tide. The mean water level for the flood (MFL) and ebb (MEL) tide is represented by the blue solid and dashed line respectively. NOTE rotor diameter to scale, TEC dimensions are not to scale.

Table 6
Sensitivity to the vertical misalignment of profiler depth bin to the proposed TEC hub-height, where each bin's mean velocity (U) is used. Values refer to the averaged velocity profile produced for each seabed instrument, where the profile for $B1$ is depicted in Fig. 12. Diff refers to the percent difference between the hub-height AEP estimate and the estimate from an depth offset.

TEC Lcoation and Type		Case 1			Case 2			Case 3		
		SW ADCP (B1)								
	D offset [m]	U [m/s]	AEP* [GWh]	Diff [%]	U [m/s]	AEP [GWh]	Diff [%]	U [m/s]	AEP* [GWh]	Diff [%]
FLOOD	2	2.01	0.82	**3.8%**	2.11	8.95	**2.1%**	2.28	19.80	**1.1%**
	1	1.99	0.81	**2.0%**	2.09	8.87	**1.2%**	2.27	19.68	**0.5%**
	HH	1.97	0.79	**0.0%**	2.08	8.76	**0.0%**	2.27	19.58	**0.0%**
	-1	1.95	0.77	**2.3%**	2.06	8.61	**1.7%**	2.26	19.44	**0.7%**
	-2	1.93	0.76	**4.5%**	2.05	8.53	**2.7%**	2.25	19.28	**1.6%**
EBB	2	2.22	1.41	**4.3%**	2.37	15.54	**2.8%**	2.49	32.56	**0.0%**
	1	2.19	1.38	**2.2%**	2.35	15.30	**1.3%**	2.49	32.58	**0.0%**
	HH	2.16	1.35	**0.0%**	2.33	15.10	**0.0%**	2.49	32.58	**0.0%**
	-1	2.13	1.32	**2.3%**	2.30	14.90	**1.3%**	2.50	32.62	**0.1%**
	-2	2.10	1.28	**5.5%**	2.28	14.70	**2.7%**	2.50	32.62	**0.1%**
		NE ADCP (B2)								
FLOOD	2	1.99	0.81	**3.6%**	2.08	8.830	**2.3%**	2.23	19.84	**0.7%**
	1	1.96	0.80	**1.9%**	2.06	8.730	**1.1%**	2.22	19.80	**0.5%**
	HH	1.94	0.79	**0.0%**	2.04	8.630	**0.0%**	2.22	19.70	**0.0%**
	-1	1.92	0.77	**2.2%**	2.03	8.520	**1.3%**	2.21	19.63	**0.3%**
	-2	1.90	0.75	**4.7%**	2.01	8.400	**2.7%**	2.20	19.58	**0.6%**
EBB	2	2.2	1.39	**2.9%**	2.21	14.10	**0.7%**	1.91	21.12	**3.2%**
	1	2.18	1.38	**2.2%**	2.21	14.20	**0.0%**	1.94	21.51	**1.3%**
	HH	2.15	1.35	**0.0%**	2.22	14.20	**0.0%**	1.95	21.80	**0.0%**
	-1	2.13	1.33	**1.5%**	2.22	14.20	**0.0%**	1.98	22.20	**1.8%**
	-2	2.11	1.30	**3.8%**	2.21	14.10	**0.7%**	2.01	22.60	**3.5%**

HH : represents 12, 18 and 34 for Case 1, Case 2 and Case 3, respectively.
D : depth.
* : represents the estimated AEP using the pre-defined power curves for a 0.1 MW and a 2 MW TEC concept.

3. Misalignment in the negative (towards sea-bed) direction (−1, −2 m) compared to a positive misalignment (towards sea-surface) has a greater impact on the estimated AEP for the flood and ebb tide across all three cases.
4. The TEC placed in the lower region (case 1) of the water column experiences greater variation in AEP under the modelled vertical misalignment, compared with cases 2 and 3.
5. Due to the greater occurrence of faster flows measured in the ebb tide compared to the flood tide, the AEP on ebb tides are greater.
6. In the upper region of the water column AEP estimates from measurements made at B_2 during the ebb tide differed by up to 3.4% when compared with measurements made at B_1.
7. For an imposed misalignment of 2 metres the AEP estimated during ebb tides from measurements at mid-depth (case 2) from B_1 and B_2 locations differed/differ by less than 1%.

4. Discussion

This work explores the sensitivity of tidal turbine power-production performance to the flow velocity reference used. The spatial variation in the flow measurements from ADCPs placed as per the IEC TS 62600-200 guidelines is found to impact the measured power curve. Furthermore, the vertical misalignment between the depth bin and the three modelled TECs of varying hub-heights affects the estimate of annual energy production.

The current velocity and direction measured by the five seabed placed ADCPs differ based on location and tidal cycle. The tidal ellipse (Fig. 3) shows the velocity magnitude (as a radius) and direction (as a compass heading transformed to a radial coordinate) in polar coordinates. The difference in the established flow direction between the five seabed ADCPs is likely due to the combination of inaccuracies in the ADCPs internal compass (due to insufficient calibration), but could also be due to localised bathymetric affects. The velocity measurements from ADCPs placed in orientation B (U_{B1} and U_{B2}) differed significantly in the ebb tide (Figs. 6b, 7b and 9b). This is likely due to a flow structure – trapped eddy – forming on the ebb tides off the local island Eday. Furthermore, ADCP placed at A_3 measured a reduced flow velocity in the upper region of the water column (Figs. 6b and 9a), suggesting the flow structure extends into this location.

The rotor-attached SB-ADP (C_1) measured velocity at hub-height along the heading of the TEC. The only ADCP found to measure similar velocities was at B_2. However, compared to the other ADCPs B_2 measurements appeared significantly lower at the hub-height of the DEEP-Gen IV, especially at lower velocity bins (<2 m s^{-1}). The discrepancy between the measured velocity at location C_1 and the five seabed ADCPs placed around the TEC may be due to several possible causes. First, as the flow decelerates upstream of the turbine (velocity reference taken at 10–12 m) the flow may already be significantly decelerated, this is commonly known as the induction zone. Secondly, the hardware and calibration, including a limit on the maximum sensor range of the SB-ADP, could cause differences in the measured velocity.

The power curves presented follow the methodology of the IEC TS 62600-200 [2]. The real-world power measurements from the DEEP-Gen IV is time-matched with the PWRA velocity calculated for the five seabed ADCPs. In addition, the velocity measured at hub-height from the SB-ADP was used to produce an additional non-PWRA power curve. During the flood tide measured by the in-line ADCP pair A_1 and A_2 (inside and close to the IEC TS target location respectively), the closer ADCP A_1 measured a slightly reduced flow. This would make the power curve appear seemingly more efficient for a developer, due to a lower velocity $\bar{U}_{A1}$ being compared against a larger velocity $\bar{U}_{A2}$ for the equivalent power measurement. The impact of this is small with a difference of ≈ 0.6% between $\bar{U}_{A1}$ and $\bar{U}_{A2}$, when the DEEP-Gen IV was operating at rated power. The difference potentially arises from a push-back on the flow when the TEC is operational or the variation in bathymetric conditions northwest of ADCP A_2 (Fig. 2).

On the contrary, the current flow does not appear to be effected by the TEC at the locations B_1 and B_2. The velocity measurements U_{B1} and U_{B2} are significantly different between the flood and ebb tide, this is evident in Fig. 8b. The velocity measured at B_1 and B_2 differed by 1.4% and 4.3% when the DEEP-Gen IV operated at rated power during the flood and ebb tide respectively (Fig. 11a and 11b), producing four different power curves (Fig. 10a and 10b). Due to the flow structure forming of the headland, the flow velocity measured at location B_2 was lower when compared with measurements from the instrument placed upstream of the turbine (A_1). This results in the power curve appearing seemingly more efficient when using measurements from instrument B_2.

The effect of ADCP placement on the estimated AEP is assessed. Based on the velocity variation between instrument locations A and B, the AEP differed by 1.2% and 2.6% when comparing ADCP pairs A_1 and A_2, and B_1 and B_2 respectively, for the flood tide measurements. For the ebb tides, the large variation between $\bar{U}_{B1}$ and $\bar{U}_{B2}$ resulted in a 7.3% difference between AEP estimates. According to the IEC TS 62600-200 the linear average velocity should be calculated when using the adjacent orientation B at equivalent water depths. For the linear average to be considered a valid approximation of the flow at the energy extraction plane, the variation in the instantaneous velocities u_{B1} and u_{B2} should be less than 10%. Fig. 9b illustrates how the mean velocity binned by increments of 0.3 m s^{-1} can vary by more than 10%, and the instantaneous velocity measurements significantly more. The study suggests that for a TEC located in the lower region of the water column (< 20 m) the adjacent orientation ADCPs can be used for power performance assessments. However, as seen in Fig. 9b, the variation in velocity upward of 20 m from the seabed exceeds the threshold required for a linear average calculation to be valid. For this reason, this instrument orientation should not be considered for a power performance assessment at this specific location for a TEC deployed in the upper region of the water column. These findings highlight the importance of studying the form of the velocity-binned depth profiles (before applying any spatial averaging and considering flood and ebb tides separately), in particular, checking for forms that suggest the presence of large-scale flow features, e.g., eddies (as shown in Figs. 8, 9 and 12). The results from implementing an IEC Type B campaign have shown at this site a significant variation in velocity on either side of the turbine location. However, this instrument layout might be suitable for power performance assessments at other test locations where the turbine and flow sensors are situated further away from flow-affecting channel features e.g., upstream headlands. The study has shown that the suitability of an IEC Type B campaign for PPA is dependent on specific turbine size and positioning in a particular channel.

The consequence of estimating AEP from flow data that might feature significant vertical misalignment between the ADCP depth bin and the rotor swept area is assessed for the DEEP-Gen IV and two further variants of horizontal axis tidal turbines. This misalignment could occur due to numerous reasons. First, differences in the estimated depth may occur due to different pressure gauge specifications and/or varying states of calibration—including human operator error or poor data traceability in terms of zero-ing of sensors. In addition, incorrect post-processing of the data and mis-matching the depth bin to the hub-height (including the blanking distance and the starting position of the first measured bin) of the turbine, can lead to inaccuracies in the measured performance. Finally, the instrument stability (pitch and roll) should be considered as this can change the depth bin between beam pairs.

The AEP was estimated using the velocity measurements at three proposed hub-heights (refer to Table 5), where a misalignment between neighbouring depth bins up to ±2 m was analysed. Results indicate the AEP was sensitive to the tidal cycle because the flood and ebb

exhibit different shear profiles. It was found that a more gradual velocity profile (typically a flood tide, refer to Fig. 12) has a lower impact on the estimated AEP, when flow data features a misalignment of 2 m. The results show (Table 6) that for regions of high vertical shear, AEP estimates become increasingly sensitive to imposed vertical misalignment.

5. Conclusion

The power performance of the DEEP-Gen IV 1 MW tidal turbine relative to five seabed placed ADCPs and one rotor-attached SB-ADP has been evaluated. These ADCPs were placed in accordance with the IEC TS 62600-200, where A_1, A_2 and A_3 are in-line and B_1, B_2 are adjacent to the TEC rotor extraction plane. The study investigates the impact on the measured power curve and AEP estimates using different flow references.

The ADCP placed closer to the TEC (A_1, $\approx$ 61 m upstream of TEC) show a slightly reduced flow when compared with the ADCP further upstream (A_2, $\approx$ 106 m upstream of TEC). This result supposedly implies that the closer instrument (A_1) produces a more efficient power curve i.e. the velocity measured is lower when compared with the time-matched velocity measured at A_2 for the equivalent power measurement. As the ADCP placed at A2 is outside the IEC TS target box, measurements are comparable with the instrument located in the box. This suggests that instruments can be deployed outside the IEC TS recommended zone and be a true representation of the flow approaching the TEC.

The ebb tide measurements revealed a significant difference in the ambient flow conditions measured at locations B_1 and B_2, this affected the AEP estimate by 7.3% when comparing the two ADCPs. The IEC TS 62600-200 guidance imposes a limit of a maximum of 10% variation between two adjacent estimates of mean velocity at a particular depth. For this study this threshold is frequently exceeded in the upper regions of the water column. This suggests that at this site, the adjacently placed instruments informed by the IEC TS 62600-200 should not be considered for a power performance assessment. It should be noted, however, that for alternate TEC designs situated lower in the water column, the rotor-adjacent measurement method may be acceptable.

The rotor-attached SB-ADP measured a reduced flow compared to the five seabed ADCPs. This is because within the measurement range (limited by the instrument's acoustic frequency, water conditions and signal strength) of the SB-ADP the flow was affected by the turbine presence and induction zone when the turbine was generating power. Our findings suggest that without further work e.g., finding and applying correction factors (which is not done in this work), this instrument configuration is unsuitable for the specific role of power performance assessment in this case. However, the SB-ADP offers several practical advantages. By integrating the instrument with the turbine, the SB-ADP, unlike stand-alone seabed setups, can be continuously powered and remotely controlled. In addition, turbine-mounted instruments can provide in-situ measurements to users in real time. This study (alongside others) has proven instruments can reliably be mounted and operated on turbines to provide in-situ measurements of current flow at turbine hub-heights. Together these advantages justify further work in this area, particularly for turbines situated high in the water column or installed on non-fixed platforms.

An investigation of AEP sensitivity to the imposed vertical misalignment of flow data to turbine rotor positioning was conducted. Three turbines were assessed, namely the ReDAPT commercial-scale tidal turbine and two further variants of horizontal axis tidal turbines, which operate in different locations of the water column with varying rotor dimensions. Results show differences in estimates of Annual Energy Production of up to 5.5%. The largest difference was found for the lowest hub-height when flow data used featured a misalignment of 2 metres with respect to the modelled rotor plane. The user of the IEC TS guidelines should realise that the placement of current sensors used in the power assessment is affected by the spatial variation of the flow (horizontal and vertical).

CRediT authorship contribution statement

Luke Evans: Conceptualization, Methodology, Formal analysis, Investigation, Writing – original draft, Revision. **Ian Ashton:** Conceptualization, Methodology, Supervision, Writing – review, Editing & revision. **Brian Sellar:** Conceptualization, Methodology, Supervision, Writing – review, Editing & revision.

Declaration of competing interest

The authors declare the following financial interests/personal relationships which may be considered as potential competing interests: This research is Funded by the EPSRC and NERC for the Industrial CDT in Offshore Renewable Energy (EP/S023933/1) and sponsored by the European Marine Energy Centre.

References

[1] S. Paboeuf, P. Yen Kai Sun, L.-M. Macadré, G. Malgorn, Power Performance Assessment of the Tidal Turbine Sabella D10 Following IEC62600-200, in: International Conference on Offshore Mechanics and Arctic Engineering, vol. 6, 2016, http://dx.doi.org/10.1115/OMAE2016-54836.

[2] International Electrotechnical Commission (IEC), PD IEC / TS 62600-200 : 2013 BSI Standards Publication Marine Energy — Wave , Tidal and Other Water Current Converters Energy Converters — Power Performance, 2013.

[3] European Communities, European Commission. Directorate General for Research, SEAFLOW, World's First Pilot Project for the Exploitation of Marine Currents at a Commercial Scale, Publications Office, 2005, p. 33, URL https://op.europa.eu/en/publication-detail/-/publication/36f20105-3d03-4324-8312-24405bdbd939.

[4] M. Harrold, P. Ouro, T. O'Doherty, Performance assessment of a tidal turbine using two flow references, Renew. Energy 153 (2020) 624–633, http://dx.doi.org/10.1016/j.renene.2019.12.052.

[5] P. Scheijgrond, A. Southall, C. Bittencourt, P. Davies, P. Mathys, G. Germain, Advancing IEC Standardisation and Certification for Tidal Energy Convertors, Tech. rep., URL https://www.icoe-conference.com/documents.

[6] G. Mccann, Implications of Site-Specific Conditions on the Prediction of Loading and Power Performance of a Tidal Stream Device, Tech. rep., 2008, URL https://www.researchgate.net/publication/228402190.

[7] R. Starzmann, I. Goebel, P. Jeffcoate, Field Performance Testing of a Floating Tidal Energy Platform-Part 1: Power Performance, Tech. rep., URL https://tethys-engineering.pnnl.gov/sites/default/files/publications/AWTEC2018-320.pdf.

[8] J. MacEnri, M. Reed, T. Thiringer, Power quality performance of the tidal energy converter, SeaGen, in: Proceedings of the International Conference on Offshore Mechanics and Arctic Engineering - OMAE, Vol. 5, 2011, pp. 529–536, http://dx.doi.org/10.1115/OMAE2011-49549.

[9] J.-C. Allo, D. Dhomé, B. Battaglia, Feedback from Sabella D10 1 MW sea trials, Tech. rep..

[10] S.G. Parkinson, W.J. Collier, Model validation of hydrodynamic loads and performance of a full-scale tidal turbine using tidal bladed, Int. J. Mar. Energy 16 (2016) 279–297, http://dx.doi.org/10.1016/j.ijome.2016.08.001.

[11] B.G. Sellar, D.R. Sutherland, Tidal Energy Site Characterisation At the Fall of Warness , Emec , Uk Energy Technologies Institute Redapt Ma1001 (Md3.8), Vol. 1001, Tech. Rep., (December) REDAPT, 2016, URL http://redapt.eng.ed.ac.uk.

[12] M. Atcheson, P. Mackinnon, B. Elsaesser, A large scale model experimental study of a tidal turbine in uniform steady fl ow, Ocean Eng. 110 (2015) 51–61, http://dx.doi.org/10.1016/j.oceaneng.2015.09.052.

[13] Z. Hameed, Y.S. Hong, Y.M. Cho, S.H. Ahn, C.K. Song, Condition monitoring and fault detection of wind turbines and related algorithms: A review, Renew. Sustain. Energy Rev. 13 (1) (2009) 1–39, http://dx.doi.org/10.1016/j.rser.2007.05.008.

[14] J. Harrison, ReDAPT MC7 . 3 Public Domain Report : Final, http://redapt.eng.ed.ac.uk/library/eti/reports/MC7.3OperationsFinalReport.pdf.

[15] J. Mcnaughton, R. Sinclair, B. Sellar, Measuring and modelling the power curve of a commercial-scale tidal turbine, in: Proceedings of the 11th European Wave and Tidal Energy Conference, (October) 2015, http://dx.doi.org/10.1017/CBO9781107415324.004, URL https://www.researchgate.net/publication/282327696.

[16] P. Jeffcoate, N. Cresswell, Field performance testing of a floating tidal energy platform - Part 2: Load performance, in: Proc. of the 4th Asian Wave and Tidal Energy Conference (AWTEC), 2018, URL https://www.researchgate.net/publication/326573036_Field_Performance_Testing_of_a_Floating_Tidal_Energy_Platform-Part_2_Load_Performance.

[17] P. Jeffcoate, R. Starzmann, B. Elsaesser, S. Scholl, S. Bischoff, Field measurements of a full scale tidal turbine, Int. J. Mar. Energy 12 (2015) 3–20, http://dx.doi.org/10.1016/j.ijome.2015.04.002, URL http://dx.doi.org/10.1016/j.ijome.2015.04.002.

[18] B.G. Sellar, D.R. Sutherland, D.M. Ingram, V. Venugopal, Measuring waves and currents at the European marine energy centre tidal energy test site: Campaign specification, measurement methodologies and data exploitation, in: OCEANS 2017 - Aberdeen, Vol. 2017-Octob, 2017, pp. 1–7, http://dx.doi.org/10.1109/OCEANSE.2017.8085001.

[19] H. Torrens-Spence, P. Schmitt, C. Frost, I. Benson, P. MacKinnon, T. Whittaker, Assessment of flow characteristics at two locations in an energetic tidal channel, in: Proceedings of the Twelfth European Wave and Tdal Energy Conference, 2017, URL https://pureadmin.qub.ac.uk/ws/portalfiles/portal/134529503/HTS_FullPaper_Version4.pdf.

[20] B.G. Sellar, G. Wakelam, D.R. Sutherland, D.M. Ingram, V. Venugopal, Characterisation of tidal flows at the european marine energy centre in the absence of ocean waves, Energies 11 (1) (2018) 1–23, http://dx.doi.org/10.3390/en11010176.

[21] Maritime, C. Agency, Guide to using the CHP bathy atlas, 2005, URL https://assets.publishing.service.gov.uk/government/uploads/system/uploads/attachment_data/file/296198/chp_bathy_atlas_guide.pdf.

[22] I. Afgan, J. McNaughton, S. Rolfo, D.D. Apsley, T. Stallard, P. Stansby, Turbulent flow and loading on a tidal stream turbine by LES and RANS, Int. J. Heat Fluid Flow 43 (2013) 96–108, http://dx.doi.org/10.1016/j.ijheatfluidflow.2013.03.010.

[23] M. Lewis, J. McNaughton, C. Márquez-Dominguez, G. Todeschini, M. Togneri, I. Masters, M. Allmark, T. Stallard, S. Neill, A. Goward-Brown, P. Robins, Power variability of tidal-stream energy and implications for electricity supply, Energy 183 (2019) 1061–1074, http://dx.doi.org/10.1016/j.energy.2019.06.181.

[24] IOOS, Manual for real-time quality control of stream flow observations (qartod) v2.1, (July) 2019, http://dx.doi.org/10.25923/sqe9-e310.

[25] RDI, Acoustic Doppler current profiler: Principles of operation, a practical primer. P/N 951-6069-00. Teledyne RD instruments, poway, California, 00, (January) 2011, p. 56.

[26] RDI, RD Instruments Acoustic Doppler Current Profilers Application Note ADCP Beam Clearance Area, Tech. rep., 2002, pp. 1–7, http://www.teledynemarine.com/Documents/BrandSupport/RDINSTRUMENTS/TechnicalResources/TechnicalNotes/ChannelMaster/FSA019.PDF.

[27] D.R.J. Sutherland, Assessment of mid-depth arrays of single beam acoustic Doppler velocity sensors to characterise tidal energy sites, 2015, URL https://era.ed.ac.uk/handle/1842/19559?show=full.

[28] J. Mcnaughton, R. Sinclair, S. Harper, D. Dobson P, P. Chesman, ReDAPT: Initial operation power curve (MC7 . 1), 2014, URL https://redapt.eng.ed.ac.uk/?p=library_redapt_reports.

[29] S. Draycott, A. Nambiar, B. Sellar, T. Davey, V. Venugopal, Assessing extreme loads on a tidal turbine using focused wave groups in energetic currents, Renew. Energy 135 (May) (2019) 1013–1024, http://dx.doi.org/10.1016/j.renene.2018.12.075.

[30] European Commission, RealTide: Advanced monitoring, simulation and control of tidal devices in unsteady, highly turbulent realistic tide environments, H2020 Programme Res. Innov. (727689) (2019) 1–45, URL https://www.realtide.eu/.